SSRG International Journal of Mechanical Engineering
ISSN: 2348-8360/ https://doi.org/10.14445/23488360/IJME-V13I2P107

Volume 13 Issue 2, 79-93, February 2026
© 2026 Seventh Sense Research Group®

Original Article

Investigation of Non-Uniform Heat Source or Sink on Bioconvection of Casson Nanofluid Over Exponential Stretching Sheet

Aparna Shendkar[1], Jagadish Tawade[2], Pradeep Janthe[3], Avinash Raut[4], Nitiraj Kulkarni[5], Nitin Ambhore[6]

[1,2,5]*Department of Mathematics, Vishwakarma University, Pune, Maharashtra, India.*
[3]*Department of Mathematics, Government First Grade College, Bidar, Karnataka, India.*
[1,4]*Department of Engineering, Sciences and Humanities, Vishwakarma Institute of Technology, Pune, India.*
[6]*Department of Mechanical Engineering, Vishwakarma Institute of Technology, Pune, India.*

[2]*Corresponding Author : jagadish.tawade@vupune.ac.in*

Received: 25 November 2025 Revised: 28 December 2025 Accepted: 27 January 2026 Published: 20 February 2026

Abstract *- The research work aims to explore the influence of non-uniform heat sources or sinks on the Bioconvection of Casson Nanofluids over a sheet that is stretched exponentially. The analysis focuses on the thermal and fluid dynamic behavior induced by the interaction between the nanofluid and microorganisms in the presence of a non-uniform thermal field, which is recognized as an important factor in improving the thermal efficiency of devices, including microbial fuel cells, bacteria-driven micromixers, microfluidic systems, enzyme biosensors, and bio-microsystems. These findings provide essential bioengineering insights to guide the development and refinement of cutting-edge technologies. Nonlinear differential equations governing the model are formulated using conservation laws, and by similarity transformation, ordinary differential equations are obtained and solved by using the MATLAB bvp4c software program, which are then plotted graphically. Results are compared using graphs. The analysis of key parameters' effects on various factors, including nanofluid velocity, temperature distribution, nanoparticle concentration, gyrotactic microorganism concentration, skin-friction, Nusselt-number, Sherwood-number, and motile-density-number, is evaluated.*

Keywords **-** *Bioconvection, Casson nanofluid, Exponential stretching sheet, Fluid dynamics, Thermal analysis.*

1. Introduction

Magnetohydrodynamics (MHD) examines how electrically conductive fluids behave when exposed to a magnetic field. As these fluids move, their conductivity generates electric currents. MHD finds applications in fusion research, engineering, MHD accelerators and power generators, and managing the transition from laminar to turbulent flow. Galtier [1] has given a brief introduction to modern Magnetohydrodynamics. Research on MHD free convection in incompressible, electrically conductive fluid flows under magnetic fields is vital in engineering and industry. It supports the development of magnetic devices, hyperthermia treatments, and techniques to reduce blood flow during surgery. It plays a crucial role in micro-MHD pumps, drug delivery, petroleum extraction, and the micro-mixing of physiological samples.

Sakiadis [2] analyzed the effect on continuous surfaces of the boundary layer and subsequently developed the basic integral and differential momentum equations for the theory of boundary layer applicable to them. Kierzenka & Shampine [3] Present the theoretical and software advancements that resulted in the creation of the BVP solver, bvp4c. This development aims to streamline the process of solving a broad range of ODEs with Boundary Value Problems (BVPs) using MATLAB. The injection and suction effect is studied by Erickson et al. [4] for a laminar boundary layer on a moving continuous flat surface. Also, the thermal and concentration boundary layers are investigated at this surface when temperature and concentration are kept constant.

Nanofluids are solid-liquid mixtures containing particles sized between 1 and 100 nanometers, comprising various nanoparticles such as metals, carbon, carbides, oxides, nitrides, and more. Choi [5] was the pioneer in reporting the properties of nanoparticles and providing experimental data to support these findings. Wong & Leon [6] highlighted various applications of nanofluids, with controllable and thermal characteristics that make them ideal for these uses. The convective instability of a nanofluid with nanoparticles and Gyrotactic Microorganisms that move in a thin horizontal layer is investigated by Kuznetsov [7].

Non-Newtonian fluids are often encountered in industrial and biological situations. One of the various forms of rheology, the Casson fluid model is well known to treat fluids possessing yield stress. The addition of nanoparticles to these fluids results in the production of Casson nanofluids, which exhibit significantly improved heat-transfer and thermal-conductivity characteristics. A fundamental understanding of the mutual influence between non-Newtonian fluid behavior and nanoparticle suspension is necessary to maximize heat transport properties in advanced applications. A typical shear-thinning fluids, such as Casson fluid, have a pretty unique viscosity profile; it is infinitely viscous at zero shear-strain and viscosity diminishes to zero with increasing shear-strain.

The Casson fluid model, which closely resembles the behaviour of blood, is the most realistic mathematical description for studying fluids having non-zero plastic dynamic viscosity. This model considers the presence of plasma and proteins and applies to substances like synthetic lubricants, paints, water, soup, jelly, blood, and tomato sauce, known as biological fluids. It is mainly relevant for the petroleum products, such as the extraction of crude oil. Because of their yield-stress characteristics, Casson fluids are very important in modeling biomechanics and polymer processing. Kamran et al. [8] examine the numerical solution of Casson Nanofluid flow over a parallel stretching surface, taking into account magnetic and Joule heating effects, with the presence of slip and thermal convective boundary conditions. Also, the numerical investigations are performed by Manvi et al [9] of Casson Nanofluids flow over porous material, where heat transfer characteristics and physical parameters of Nanofluids are examined.

The stretching velocity increases with the distance between two points on the sheet. When a sheet is stretched, it undergoes exponential stretching. This method has numerous technological applications in industries, such as aerodynamic production of plastic sheets, fluid film condensation, crystal growth, chemical processing, metallic sheet cooling, heat transfer systems, and the manufacturing of glass and polymers. Naseem & Kasana [10] studied Thermal Radiation and Magnetohydrodynamics effects on the aiding and opposing flow of $Al_2O_3 - Cu\,/H_2O$ hybrid nanofluid over a porous exponentially stretching surface, considering a stagnation point, non-uniform heat source/sink, and convective boundary conditions.

Shankar et al. [11] considered the three-dimensional MHD flow of Casson fluid over a stretching sheet in a non-Darcy porous medium subject to a heat source/sink. The influence of Cattaneo-Christov heat flux and Joule effect is also taken into account. Babu et al. [12] investigate second-order chemical reaction effects on steady two-dimensional MHD flow of conducting Casson fluid in a stratified porous medium over an exponentially stretching sheet.

Microscopic suspended particles, such as algae and bacteria, that form natural patterns are called Bioconvection, which is driven by a density gradient caused by collective swimming, leading to thermoscopic convective flow. Waqas et al. [13] conducted a simulation for a burger nanofluid with an exponential heat source/sink. The finding showed that temperature distribution increases as the temperature ratio parameter rises, but it decreases as the Prandtl number increases.

Bioconvection has many uses, including Biofuel-Producing Reactors, Solar Cells, Bio-Microbial Fuel Cells , and Syn-Gas production in the renewable energy sector. Moreover, Bioconvection finds application in engineering and geology (for example, microsystems, drilling technologies, polymer science), robotics (disturbing the benthic ecosystem might be a matter of significant importance in robotic prototyping), and oil extraction and its refining. Kuznetsov and Avramenko [14] pointed out that bioconvection development enhances the mixing process and retards the particle settling, with high relevance in pharmaceutical problems.

The non-uniform heat sources/sinks are highly influential for precise modeling and examination of complex thermal systems in MHD research. This method clearly facilitates a better understanding of heat transfer and fluid mechanics, in addition to the optimization and performance enhancement for a variety of applications. Li et al. [15] examined the influence of a non-uniform heat source/sink and viscous dissipation on the Magnetohydrodynamic flow of Casson fluid containing nanoparticles passing over a porous, permeable sheet. These are surface transport phenomena called heat flux, skin friction, and mass flux, aside from the three boundary layers above.

Xu et al. [16] have investigated the new aspects of the induced magnetic field in the bio-convection patterns of third-order nanofluids with impressive impact on activation energy and non-uniform heat source/sink conditions. Kumar et al. [17] investigate the effects of a magnetic field parameter, thermal radiation, and a non-uniform heat source or sink on two-dimensional unsteady nanofluid flow over a permeable exponential stretching surface.

Sharanayya and Suresh [18] carried out a numerical study for the impact of magnetic ohmic heating and viscous dissipation on the steady-state flow of Casson Nanofluid past a porous medium over a stretching sheet with heat source/sink effects. They have taken into account Brownian motion and thermophoresis effect, as well as Soret and chemical reaction effects. [19] Mahes et al. studied the effect of radiation on MHD couplestress Hybrid Nanofluid Ooze flow through a porous sheet with dissipation. Polu et al. [20] discuss a numerical solution for heat and mass transfer in time-dependent hydromagnetic boundary layer flow of a viscous fluid over an exponentially inclined stretching sheet with viscosity heating, thermal radiation, non-uniform energy generation or absorption, and different slip. Sankari et al. [21] analyze the double stratification effects on the steady 2-D MHD Casson Nanofluid over an exponentially porous stretching sheet, taking into account features such as thermophoresis and Brownian motion, for a simple explanation of nanoparticles used.

Sankari et al. [22] investigated hydromagnetic Bioconvection of a Casson nanofluid over an exponentially stretching sheet with activation energy and motile microorganisms by the homotopy analysis method. They found that key parameters have a significant influence on the flow and heat transfer. Also illustrated that Gyrotactic Microorganisms enhance the bioconvective transport and provided semi-analytical insights into non-Newtonian nanofluid heat transfer for engineering applications. Vinod, Y., et al [23] studied advanced numerical techniques, particularly the wavelet method, which numerically analyzes MHD flow boundary layers, Casson fluids, radiation effects, and heat source/sink effects over an exponentially stretching surface.

Though many investigations have been carried out on MHD nanofluid flow and Bioconvection separately, the combined effect of MHD effects, Casson fluid rheology characteristics, Bioconvection of motile microorganisms, an exponential stretching sheet, and non-uniform heat source or sink has not been well studied. Motivated by such research voids, the objective of this study is to examine the effect of non-uniform heat sources or sinks on Casson Nanofluid Bioconvection over an exponentially stretching sheet.

Appropriate similarity transformations are employed to convert the resulting nonlinear partial differential equations into a system of ordinary differential equations that are solved numerically. The effects of some important dimensionless parameters on velocity, temperature, nanoparticle concentration, and microorganism density distributions are discussed in detail, which will be helpful for the design of MHD thermal/bioengineering systems.

In this research, the space- and temperature-dependent internal heat generation affects the Magnetohydrodynamic Casson Nanofluid Bioconvection boundary layer flow over an exponentially stretching surface. The novelty of our study lies in using an exponentially decaying heat source in the heat equation, unlike previous studies that used a constant source.

The effects of non-Newtonian Fluids, Joule Heating, Viscous Dissipation, Nonlinear Radiation, Brownian Motion, Thermophoresis, and Microorganisms. A numerical solution using the bvp4c solver is obtained. To our knowledge, this type of study has not been reported in the literature.

2. Materials and Methods

2.1. Analysis of Non-Optimized Design

Figure 1 depicts the geometry of the current investigation. A 2D Casson Nano liquid motion across an exponentially elongating sheet is considered.

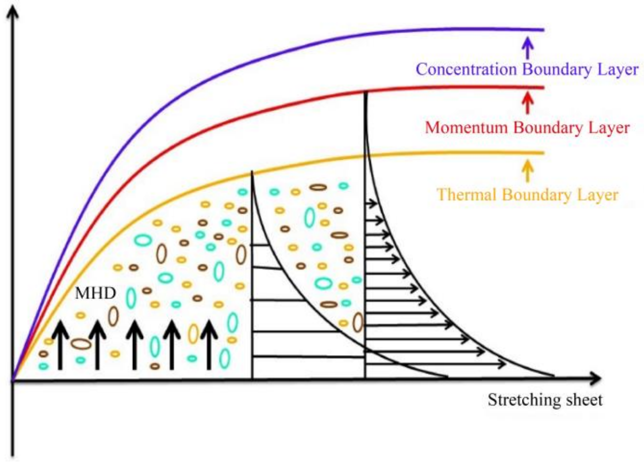

Fig. 1 Geometry analyzed

The Bioconvection of Casson Nanofluids for the considered sheet is governed by the following equations (dimensional coupled nonlinear equations) [16-18].

$$\frac{\partial \mathrm{you}}{\partial \mathrm{x}} + \frac{\partial \mathrm{v}}{\partial \mathrm{y}} = 0 \tag{1}$$

$$\mathrm{u}\frac{\partial \mathrm{u}}{\partial \mathrm{x}} + \mathrm{v}\frac{\partial \mathrm{u}}{\partial \mathrm{y}} = \nu\left(1+\frac{1}{\beta}\right)\frac{\mu_{\mathrm{nf}}}{\rho}\frac{\partial^2 \mathrm{you}}{\partial \mathrm{y}^2} - \frac{\sigma B^2}{\rho}\mathrm{u} - \nu\left(1+\frac{1}{\beta}\right)\frac{\mathrm{you}}{k'} + \frac{1}{\rho}\left[g\beta_p(T-T_\infty)(1-C_\infty) - g\left(\rho_p-\rho_f\right)(C-C_\infty) - g\gamma\left(\rho_m-\rho_f\right)(N-N_\infty)\right] \tag{2}$$

$$\mathrm{u}\frac{\partial \mathrm{T}}{\partial \mathrm{x}} + \mathrm{v}\frac{\partial \mathrm{T}}{\partial \mathrm{y}} = \alpha\frac{\partial^2 \mathrm{T}}{\partial \mathrm{y}^2} - \frac{1}{\rho C_p}\frac{\partial q_r}{\partial \mathrm{y}} + \frac{\nu}{C_p}\left(1+\frac{1}{\beta}\right)\left(\frac{\partial \mathrm{you}}{\partial \mathrm{y}}\right)^2 + \frac{\sigma {B_0}^2 u^2}{\rho C_p} + \nu\left(1+\frac{1}{\beta}\right)\frac{u^2}{k' C_p} + \left[D_B\frac{\partial C}{\partial y}\frac{\partial T}{\partial y} + \frac{D_T}{T_\infty}\left(\frac{\partial \mathrm{T}}{\partial \mathrm{y}}\right)^2\right] + \frac{q'''}{(\rho C_p)_{\mathrm{nf}}} \tag{3}$$

$$u\frac{\partial C}{\partial x} + v\frac{\partial C}{\partial y} = D_B\frac{\partial^2 \mathrm{C}}{\partial \mathrm{y}^2} + \frac{D_T}{T_\infty}\frac{\partial^2 \mathrm{T}}{\partial \mathrm{y}^2} - (K_r)^2(C - C_\infty)\left(\frac{\mathrm{T}}{T_\infty}\right)^n exp\left(\frac{-Ea}{kT}\right) \tag{4}$$

$$u_a\frac{\partial N}{\partial x} + \nu_b\frac{\partial N}{\partial y} + \mathrm{b}W_c\frac{\partial}{\partial x}\left(\frac{n}{\Delta C}\frac{\partial C}{\partial y}\right) = D_m\frac{\partial}{\partial y}\left(\frac{\partial N}{\partial y}\right) \tag{5}$$

Where u and v are velocity components in the direction x and y, respectively, while T signifies the temperature of the liquid.

The equivalent boundary restrictions are:

$$u = U = U_0 e^{x/L}, v = -V(x) = -V_0 e^{x/L},$$

$$T = T_w(x) = T_0 + be^{x/2L}, \quad C = C_w(x) = C_0 + me^{x/2L}, \quad N = N_w(x) = N_0 + pe^{x/2L}, at\ y = 0 \tag{6}$$

$$u \to 0, T = T_\infty(x) = T_0 + ce^{x/2L}, \quad C = C_\infty(x) = C_0 + ne^{x/2L}, \quad N = N_\infty(x) = N_0 + qe^{x/2L}, \quad as\ y \to \infty \tag{7}$$

Where, U_0 −Reference velocity, suction velocity, $V(x) > 0$ and blowing velocity, $V(x) < 0$.
$V_0 > 0$, initial suction strength and $V_0 < 0$, initial blowing strength.

Now, using similarity transformation as follows:

$$\eta = \sqrt{\frac{U_0}{2\nu L}}\ e^{x/2L} y, u = U_0\ e^{x/2L} f'(\eta),$$
$$v = -\sqrt{\frac{\nu U_0}{2\nu L}}\ e^{x/2L}\{f(\eta) + \eta f'(\eta)\}$$
$$\phi(\eta) = \frac{C - C_\infty}{C_w - C_0}, \qquad \theta(\eta) = \frac{T - T_\infty}{T_w - T_0},$$
$$\chi(\eta) = \frac{N - N_\infty}{N_w - N_0} \tag{8}$$

Here, η - similarity variable and $f(\eta)$ - dimensionless stream function

$$\left(1 + \frac{1}{\beta}\right) f''' + ff'' - 2f'^2 - Mf' - Kpf' + \omega(\theta - N_r\,\phi - Rb\chi) = 0 \tag{9}$$

$$\left(1 + \frac{4}{3}R\right)\theta'' + Pr(f\theta' - f'\theta - Tsf' + Q\theta + N_b\,\phi'\theta' + N_t(\theta')^2) + \mathrm{Pr}\,Ec\left(1 + \frac{1}{\beta}\right)(f'')^2 + \mathrm{Pr}\,Ec\,Mf'^2 + \mathrm{Pr}\,Ec\,Kpf'^2 + A^* f' + B^*\theta = 0 \tag{10}$$

$$\phi'' + Sc(f\,\phi' - f'\,\phi) - Csf' - A\,\phi(1 + \delta\theta)^m exp\left(\frac{-E}{1+\delta\theta}\right) + \frac{N_t}{N_b}\theta'' = 0 \tag{11}$$

$$\chi'' + Sb(\chi' f - \chi f) - SbMsf' - P_e[\,\phi''(\chi + \Omega) + \phi'\chi'\,] = 0 \tag{12}$$

Equivalent boundary conditions given by,

$$f = S, \quad f' = 1, \quad \theta = 1 - Ts, \quad \phi = (1 - Cs), \quad \chi = (1 - Ms), \quad as,\ \eta \to 0$$
$$\theta \to 0, \quad f' \to 0, \quad \phi \to 0, \quad \chi \to 0, \quad as\, \eta \to \infty \tag{13}$$

Here, prime denotes derivatives wrt η.

Dimensionless flow parameters are as follows:

$K_p = \frac{2L\nu}{k^* U_0}$ It is a porous structure.

$P_r = \frac{\nu}{\alpha}$ is the Prandtl number

$M = \frac{2\sigma B_0{}^2}{\rho U_0 e^{x/L}}$ is the magnetic parameter

$S_c = \frac{\nu}{D}$ is the Schmidt number

$C_s = \frac{n}{m}$ is the chemically stratified structure

$Q = \frac{2LQ_0}{U_0 \rho \mathrm{C_p}}$ is a heat source parameter

$Ts = \frac{c}{b}$ is the thermally stratified structure

$S = \frac{V_0}{\sqrt{\frac{\nu U_0}{2L}}}$ is the blowing constraint

$\omega = \frac{(1-C_\infty)\beta g(T_w - T_0)2L}{U_0{}^2}$ is the mixed convection constraint

$R_b = \frac{(\rho_p - \rho_f)(N_w - N_\infty)}{(1-C_\infty)\beta\rho(T_w - T_\infty)}$ is the bioconvection Rayleigh number

$Nr = \frac{(\rho_p - \rho_f)(C_w - C_\infty)}{(1-C_\infty)\beta\rho(T_w - T_\infty)}$ is Buoyancy ratio

$N_b = \frac{\tau D_B(C_w - C_\infty)}{\nu T_\infty}$ is the Brownian factor

$Nt = \frac{\tau D_T(T_w - T_\infty)}{\nu T_\infty}$ is the thermophoresis diffusion

$R = \frac{4\sigma^* T_\infty{}^3}{k^* K}$ is the radiation

$Sb = \frac{\nu}{D_m}$ is Schmidt number (Bioconvection)

$P_e = \frac{bW_n}{D_n}$ is the Peclet number

$E = \frac{E_a}{kT_\infty}$ is Non-dimensional energy activation

$Sh_x = \frac{xJ_w}{D(C_w - C_\infty)}$ is the local Sherwood number

$A = \frac{2k_r{}^2 L}{U_0}$ is a Dimensionless reaction rate

$Nn_x = \frac{xq_n}{D_m(N_w - N_\infty)}$ is the Motile density number

$Cf_x = \frac{\tau_w}{\rho U^2}$ is the drag force factor

$\mathrm{Nyou_x} = \frac{\mathrm{xq_w}}{\mathrm{k(T_w - T_\infty)}}$ is the local Nusselt number

$\tau_w = 2\mu\left(\frac{\partial u}{\partial y}\right)_{y=0}$ is shear stress

$q_w = -k\left(1 + \frac{4R}{3}\right)\left(\frac{\partial T}{\partial y}\right)_{y=0}$ is heat flux

$J_w = -D\left(\frac{\partial C}{\partial y}\right)_{y=0}$ is mass flux

$\mathrm{q_n} = -\mathrm{D_m}\left(\frac{\partial \mathrm{N}}{\partial \mathrm{y}}\right)_{\mathrm{y}=0}$ at the surface

Equation (7) is used to determine the rates of mass transference, wall heat, and drag force coefficient (non-dimensional)

$$f''(0) = \frac{C_f}{\sqrt{\frac{2}{R_e}}\sqrt{\frac{x}{L}}}, \quad -\theta'(0) = \frac{Nu(1 - T_s)}{\sqrt{\frac{2}{R_e}}\sqrt{\frac{x}{L}}},$$
$$-\varphi'(0) = \frac{Sh(1 - C_s)}{\sqrt{\frac{2}{R_e}}\sqrt{\frac{x}{L}}},$$
$$-\chi'(0) = \frac{Nn(1 - M_s)}{\sqrt{\frac{2}{R_e}}\sqrt{\frac{x}{L}}}$$

2.2. Numerical Analysis

By using MATLAB-based solver, the bvp4c method, the boundary value problems involving ODEs are solved. For the transformed equations governing heat transfer and boundary layer flow, a numerical solution was obtained using bvp4c. It is particularly suitable for nonlinear, coupled ODEs with multi-point boundary conditions.

The ODEs (9) – (12), along with boundary conditions (13), are converted to first-order simultaneous equations, as follows.

$$\left.\begin{matrix} f(1) = f,\ \ f(2) = f',\ \ f(3) = f''; \ f(4) = \theta,\ \ f(5) = \theta'\ ; \\ f(6) = \phi,\ \ f(7) = \phi'\ ; \ f(8) = \chi,\ \ f(9) = \chi'\ ; \end{matrix}\right\} \tag{14}$$

$$f''' = \frac{-1}{\left(1+\frac{1}{\beta}\right)}\{f(1)f(3) - 2f(2)^2 - Mf(2) - K_P f(2) + \omega(f(4) - N_r\phi - Rb\, f(8)\} \tag{15}$$

$$\theta'' = -\frac{1}{\left(1+\frac{4}{3}R\right)}\Big[Pr\{f(1)f(5) - f(2)f(4) - Tsf(2) + Qf(4) + N_b f(7)f(5) + N_t f(2)^2\} + PrEc\left(1+\frac{1}{\beta}\right)f(3)^2 + \mathrm{Pr}\, Ec\ \ Mf(2)^2 + Pr\ Ec\ Kp\ f(2)^2 + A^* f(2) + B^* f(4)\Big] \tag{16}$$

$$\phi'' = Sc(f(2)f(7) - f(2)f(6) - Csf(2) - A\, f(6)(1 + \delta\, f(4))^m\, exp\left(\frac{-E}{1+\delta\, f(4)}\right) + \frac{N_t}{N_b}\theta'' \tag{17}$$

$$\chi'' = Sb\{f(9)f(1) - f(8)f(1)\} - Sb\, M_s f(1) - P_e[\,\phi''(f(8) + \Omega) + f(9)f(7)] \tag{18}$$

We have applied boundary conditions to the problem as follows:

$$f(1) = S,\ f(2) = 1,\ f(4) = 1 - Ts,\ f(6) = (1 - Cs)\,,\ f(8) = (1 -\ Ms)\ \ at\ \eta \to 0$$

$$f(2) \to 0, f(4) \to 0,\quad f(6) \to 0,\quad f(8) \to 0\ \ as, \eta \to\ \infty \tag{19}$$

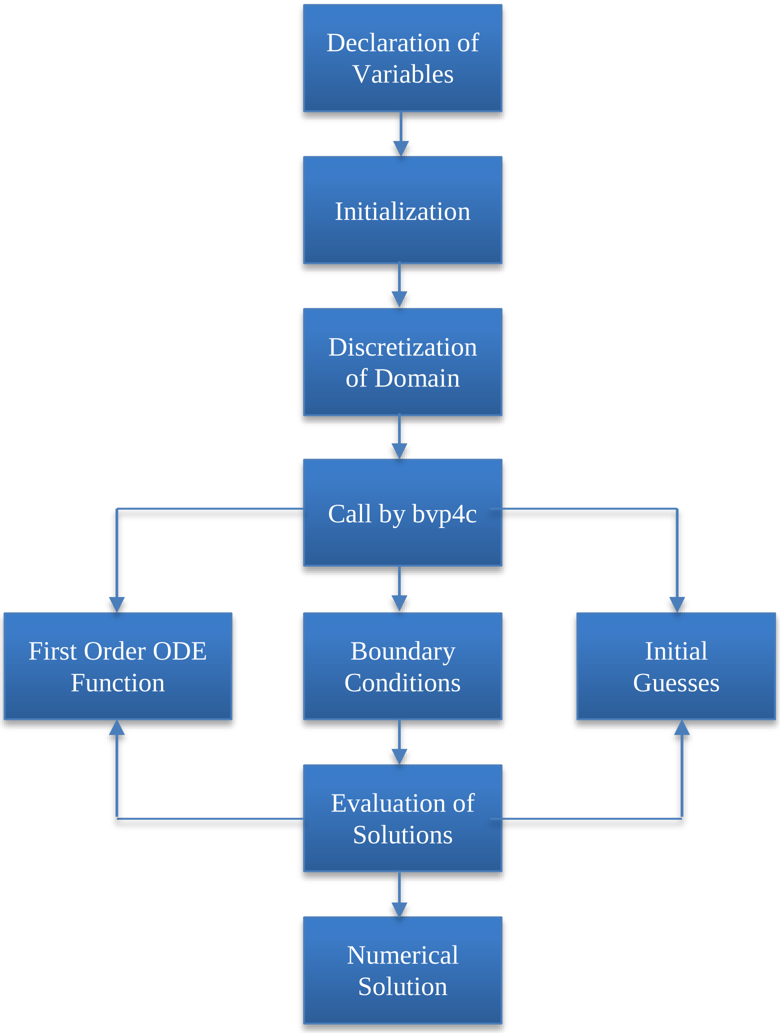

Fig. 2 Solution methodology

3. Results and Discussion

Numerical results are summarised in Tables 1-4 for local gradients of various physical quantities, showcasing variations with prominent parameters.

Table 1. Numerical results for -$f''(0)$ against the various values of the M, b, K, x, Nr, Rb, and S structures

M	β	K_p	ω	N_r	R_b	S	Sankari et al. [22]-$f''(0)$	Obtained results
0.5							0.9723	0.974295
1.0							1.0223	1.022439
1.5							1.0723	1.072751
	0.5						0.9923	1.004301
	1.0						1.0923	1.124293
	1.5						1.1256	1.115672
		0.5					0.2023	0.204671
		1.0					0.2523	0.252459
		1.5					0.3023	0.318652
			0.1				0.1941	0.189441
			0.2				0.1932	0.196396
			0.3				0.1923	0.216583
				0.1			0.1815	0.186936
				0.2			0.1842	0.186491
				0.3			0.1869	0.193269
					0.1		0.1815	0.204692
					1.1		0.2085	0.280865
					2.1		0.2355	0.239532
						0.1	0.1896	0.175096
						0.3	0.2096	0.21386
						0.5	0.2296	0.22965

Table 2. Numerical results for $\theta'(0)$ against the various values of the R, Pr, Q, Ts, Nb, Nt, and Ec structures

R	P_r	Q	E_c	N_b	N_t	T_s	Sankari et al. [22] $\theta'(0)$	Obtained results
0.1							0.5221	0.522342
0.4							0.4861	0.486132
0.7							0.4501	0.450235
	1.0						0.7068	0.707432
	2.0						0.6635	0.663501
	3.0						0.6203	0.620923
		0.1					0.2814	0.354217
		0.5					0.2478	0.256743
		1.0					0.1983	0.320964
			0.1				0.6738	0.673838
			0.2				0.5739	0.574632
			1.1				0.4742	0.452142
				0.1			0.2754	0.302754
				0.6			0.2411	0.229411
				1.1			0.2077	0.201077
					0.1		0.2945	0.349845
					0.6		0.2611	0.263911
					1.1		0.2277	0.224327
						0.3	0.3686	0.3686
						0.4	0.3796	0.3796
						0.5	0.3906	0.3906

Table 3. Numerical results for $\phi'(0)$ against the various values of the Sc, A, Cs, and E structures

S_c	A	E	C_s	Sankari et al. [22] $\phi'(0)$	Present results
0.1				0.72775	0.727651
0.6				0.78225	0.782240
1.1				0.83675	0.83732
	0.1			0.70794	0.70854
	1.1			0.63934	0.645216
	2.1			0.57074	0.570823
		0.1		0.69788	0.697975
		1.1		0.71388	0.713875
		2.1		0.72988	0.735386
			0.2	0.6909	0.691564
			0.3	0.6919	0.692321
			0.4	0.5139	0.514563

Table 4. Numerical results for $\chi'(0)$ against the various values of the Pe, Sb, Ms, and ′Ω structures

P_e	S_b	′Ω	M_s	Sankari et al. [22] $\chi'(0)$	Obtained results
0.2				0.8506	0.850451
0.3				0.8673	0.867310
0.4				0.8893	0.889461
	0.1			0.8339	0.833621
	0.3			0.8486	0.848612
	0.5			0.8632	0.863259
		0.1		0.8304	0.830967
		1.1		0.8393	0.839306
		2.1		0.8493	0.849731
			0.1	0.9005	0.900954
			0.2	0.9015	0.901511
			0.3	0.8051	0.805185

The values of parameters M, b, K, Rb, and w are shown to influence the skin friction coefficient as given in Table 1. Skin friction increases with M, b, K, S, and Rb and decreases with w and Nr. The effect of R, Pr, Q, Ec, Nb, Nt, and Ts on convective heat transfer rate is presented in Table 2. Heat transfer is found to increase with Pr, Ts, but decrease with R, Q, Ec, Nb, and Nt. The effects of A, Sc, E, and Cs on Sh are summarized in Table 3. The increase of A and Cs still led to a decrease in mass transfer rate, while E and Sc raised it. The influence of X, Pe, Ms, and Sb on the dispersion of microorganisms is given in Table 4. A rise in X, Pe, and Sb will raise the microorganism rate, and a rise in Ms will lower the rate of microorganism.

Figure 3 shows that as magnetic field strength increases, the resulting Lorentz force reduces the overall velocity gradient. However, due to the induced electric field accelerating effect, the velocity near the stretching sheet increases. It is used in electromagnetic flow meters, cooling systems for nuclear reactors, plasma control, and metallurgical processes, where flow speed control is essential, known as the damping effect. Figure 4 demonstrates that an increase in the Casson fluid β parameter reduces the velocity of fluid as well as the velocity gradient due to an increase in yield stress. This parameter shows the viscoplastic nature of fluid as well as shear-thinning effects. This is particularly critical in scenarios such as blood flow modelling and transport of polymeric fluid.

Plot 5 identifies the effect of porosity on fluid velocity. It shows that porosity raises resistance to flow, augmenting damping to flow and reducing fluid velocity. Lower permeability also limits motion, leading to slower flow and increased surface shear stress. The buoyancy ratio is a dimensionless quantity that exhibits the balance between thermal and solutal buoyancy forces. Figure 6 shows how the buoyancy ratio structure affects the velocity. As the buoyancy ratio decreases, fluid velocity increases. A higher ratio indicates buoyancy-dominated flow. When the particles and fluid densities are considerably different, the Buoyancy effect might rise. The particles may either float or sink, causing changes in their stability, and the velocity of nanofluid flow may be disturbed. This parameter is helpful in analysing fluid behaviour in systems like heat exchangers, chemical reactors, and MHD applications.

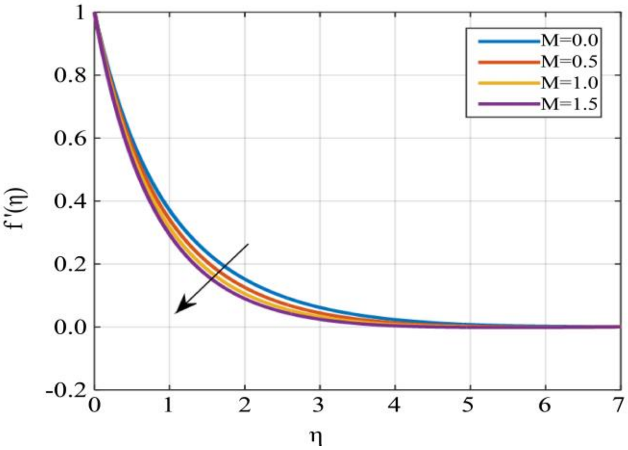

Fig. 3 Variations of M to $f'(\eta)$

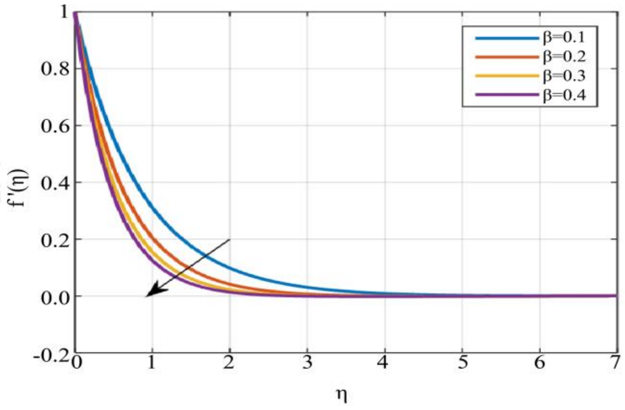

Fig. 4 Variations of β to $f'(\eta)$

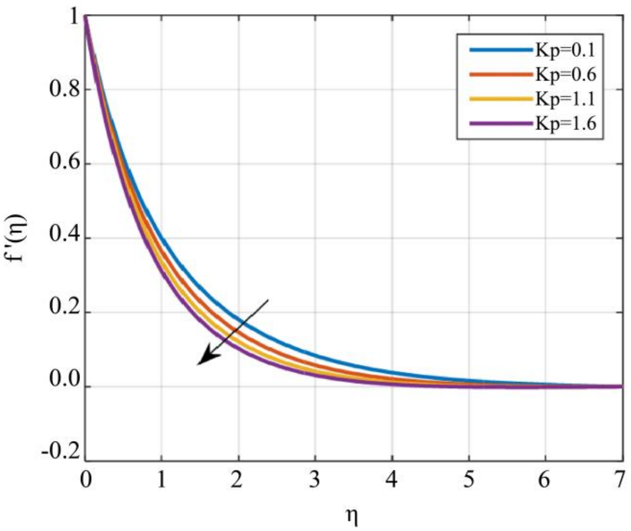

Fig. 5 Variations of *kp* to $f'(\eta)$

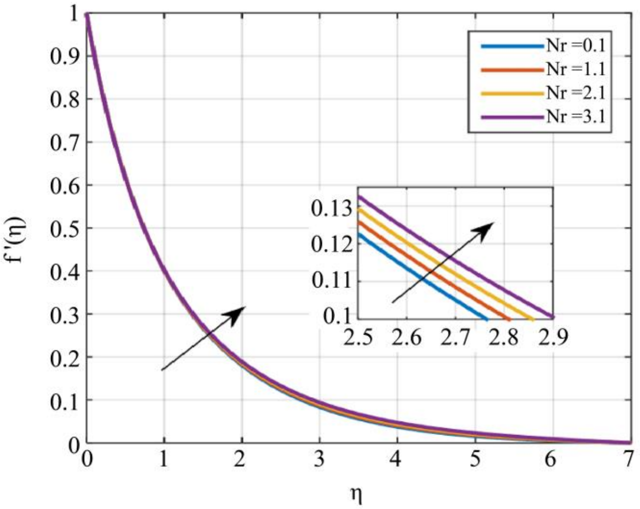

Fig. 6 Variations of Nr to $f'(\eta)$

As per Figure 7, an increase in the Rayleigh number(Bioconvection) decreases the velocity gradient, enhancing buoyancy forces relative to viscosity, which leads to an alteration in the local flow retardation as well. Higher Rb values, indicating dominance of buoyancy-driven convection, show more intense fluid motion.

Figure 8 demonstrates how mixed convection influences flow velocity. As the parameter 'ω' increases, the velocity fluctuates on both surfaces. Elevated values of w signify stronger inertial dominance, resulting in increased fluid velocity; thus, it shows the correlation between inertial and viscous forces.

Figure 9 explains the impact of suction on the velocity gradient over an exponentially stretching sheet. This effect occurs due to the interaction between the outer flow and the boundary layer on the adjacent sheet. Suction removes fluid from the boundary layer such that it becomes thinner and, in turn, decreases the velocity of the fluid. Blowing, on the other hand, displaces the heated fluid from the wall. This minimizes the effect of viscosity on the fluid such that the fluid is able to accelerate, which leads to an increase in velocity.

Figure 10 distinctly illustrates the effect on the temperature gradient. Porosity acts because it has the power to regulate multiple interrelated factors in porous materials. Porosity's extent dictates the flow of heat through the material by acting on multiple significant factors: fluid motion (liquids or gases), the efficiency of heat transfer, thermal conductivity, the accessible surface area for heat exchange, and fluid flow speed. Knowing how porosity influences these processes is critical to precisely predicting and controlling temperature gradients in porous materials, which pervade a multitude of applications.

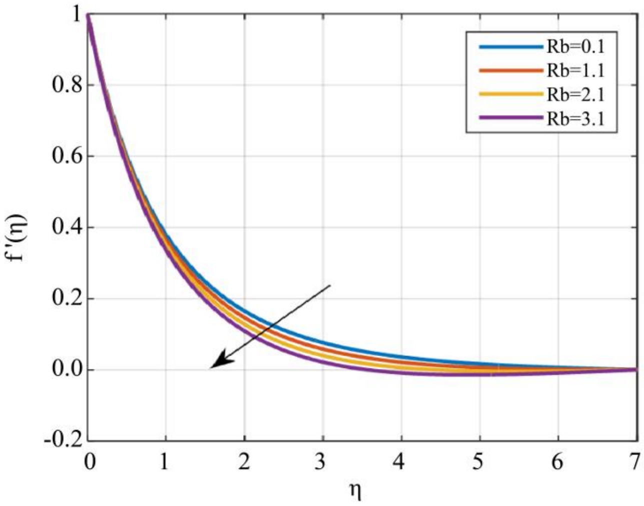

Fig. 7 Variations of Rb to $f'(\eta)$

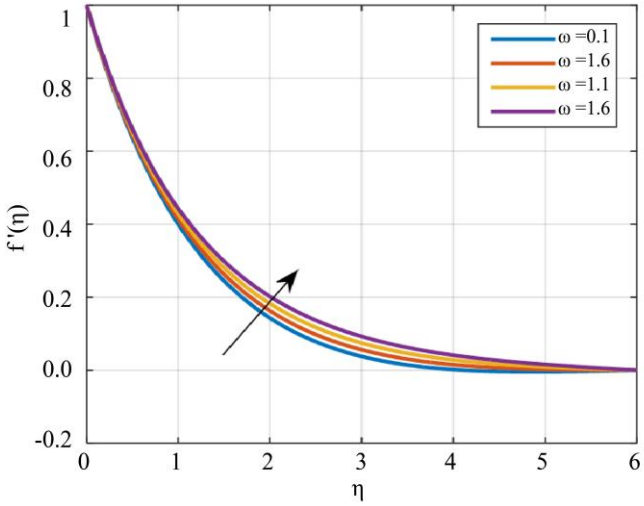

Fig. 8 Variations of ω to $f'(\eta)$

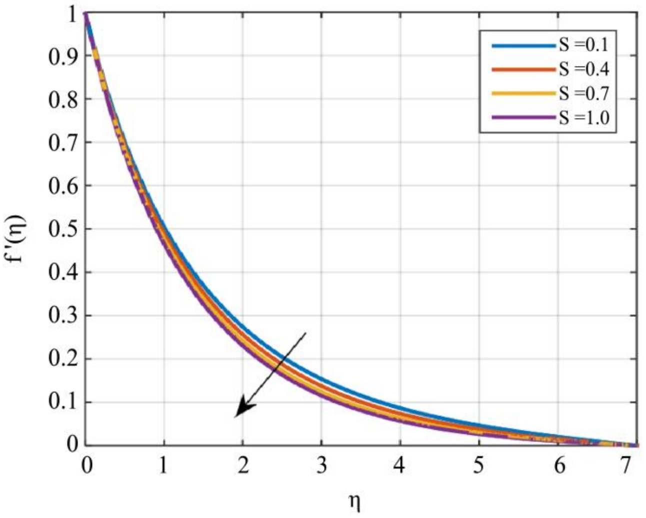

Fig. 9 Variations of S to $f'(\eta)$

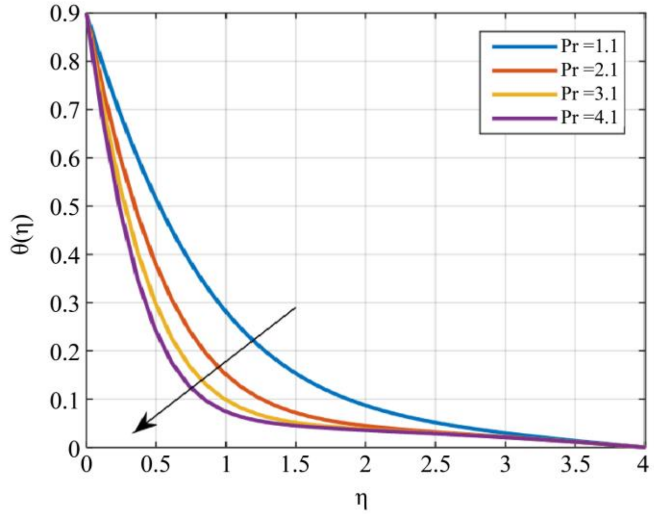

Fig. 12 Variations of Pr to $\theta(\eta)$

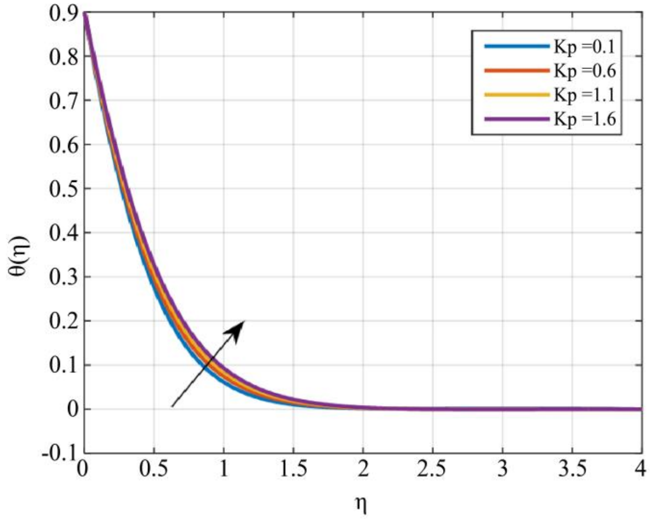

Fig. 10 Variations of *Kp* to $\theta(\eta)$

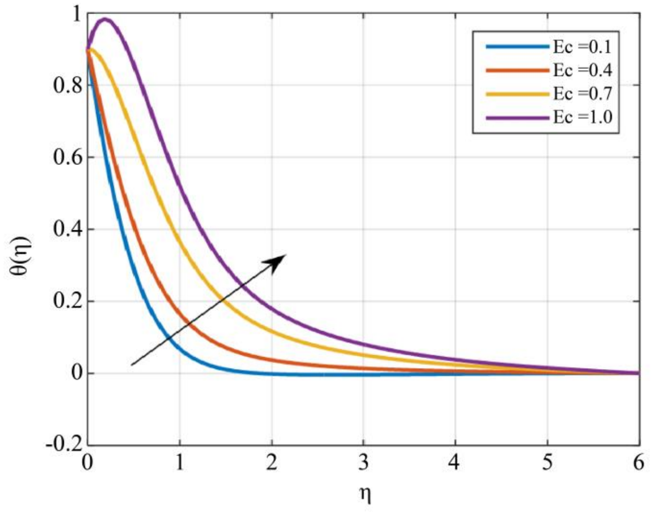

Fig. 13 Variations of Ec to $\theta(\eta)$

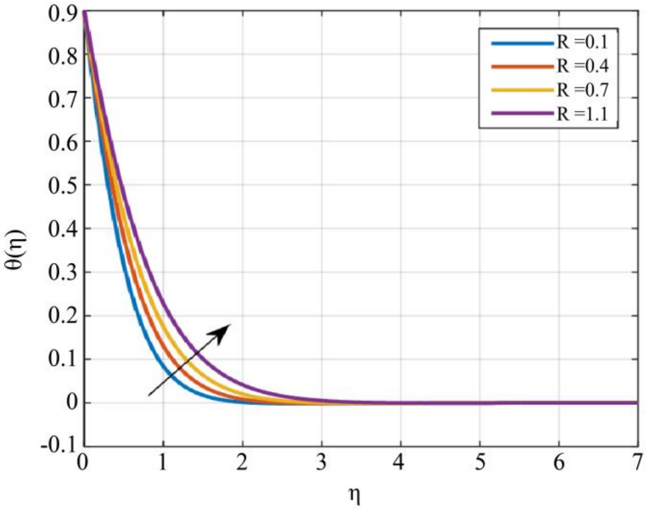

Fig. 11 Variations of R to $\theta(\eta)$

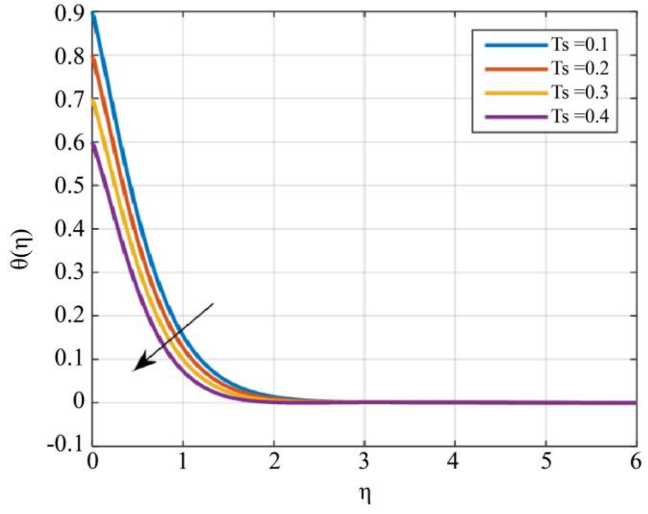

Fig. 14 Variations of Ts to $\theta(\eta)$

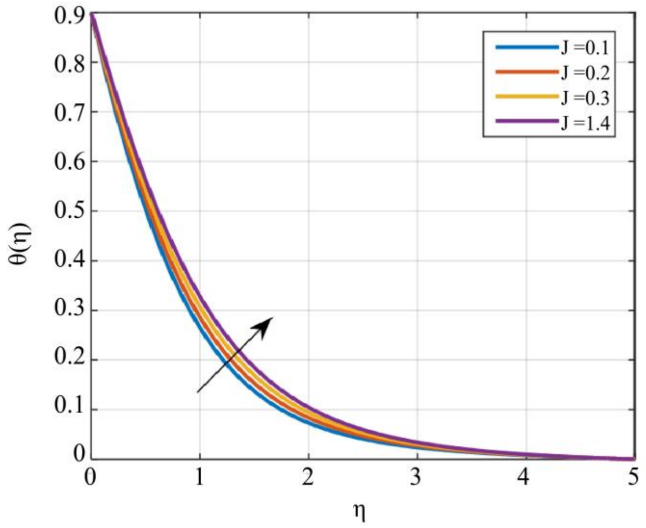

Fig. 15 Variations of J to θ(η)

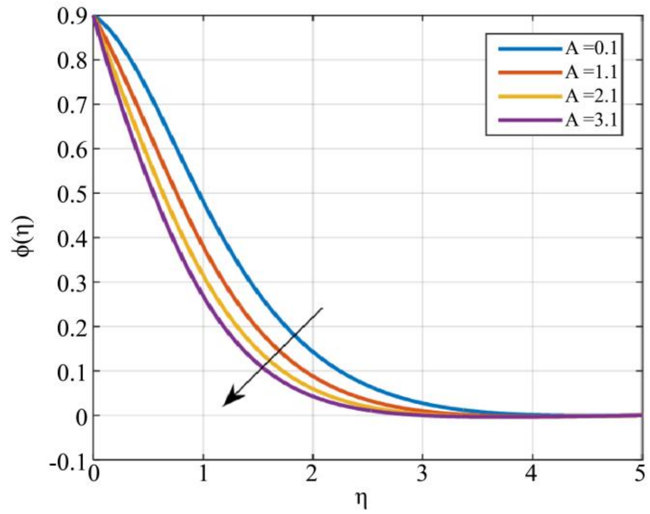

Fig. 18 Variations of A to ϕ(η)

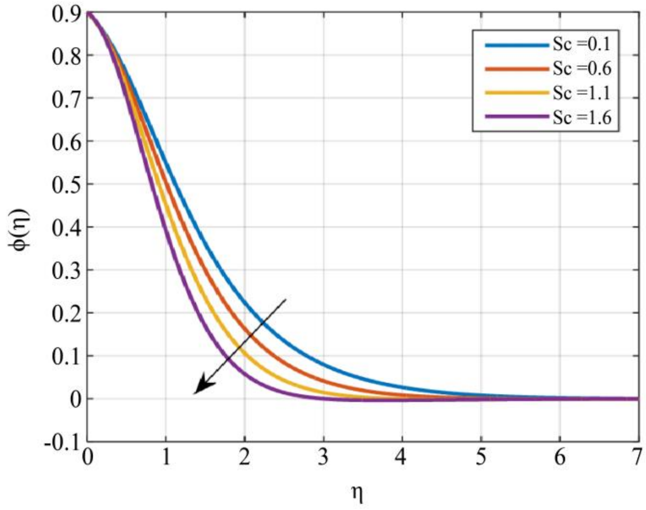

Fig. 16 Variations of Sc to ϕ(η)

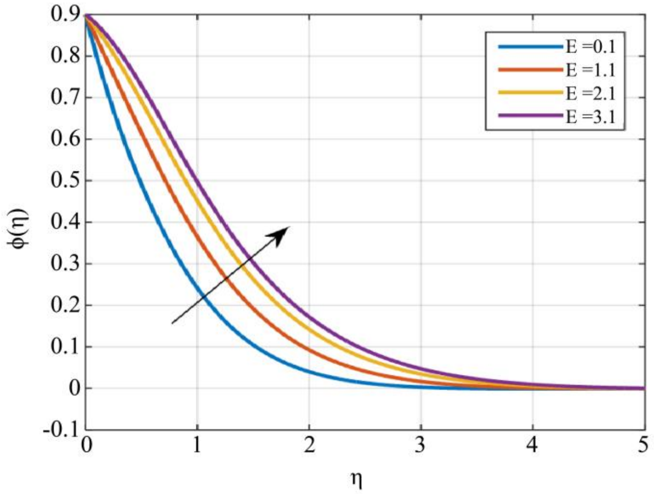

Fig. 19 Variations of E to ϕ(η)

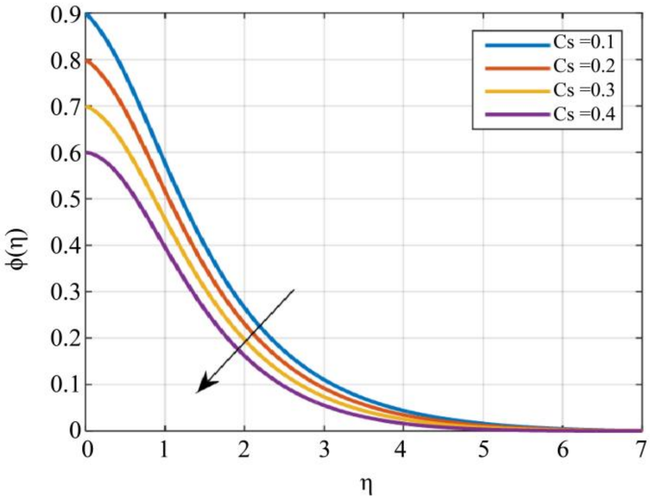

Fig. 17 Variations of Cs to ϕ(η)

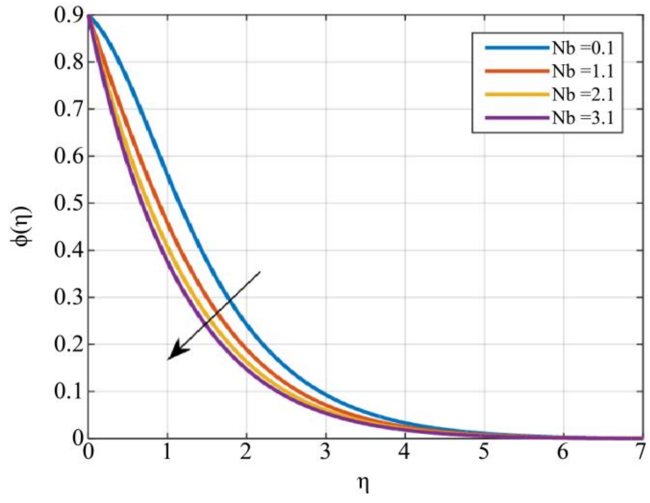

Fig. 20 Variations of Nb to ϕ(η)

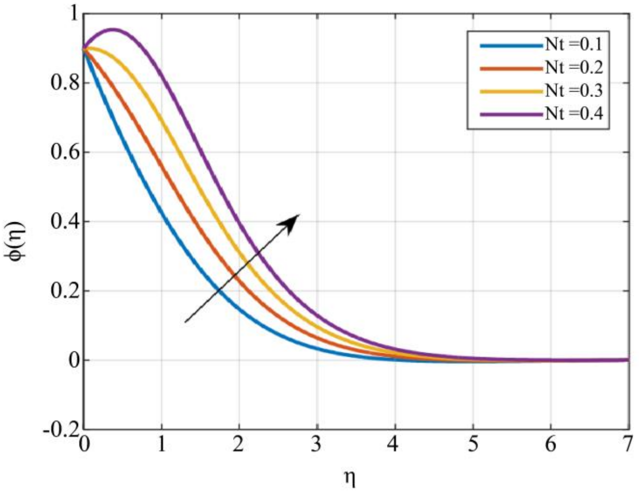

Fig. 21 Variations of Nt to $\phi(\eta)$

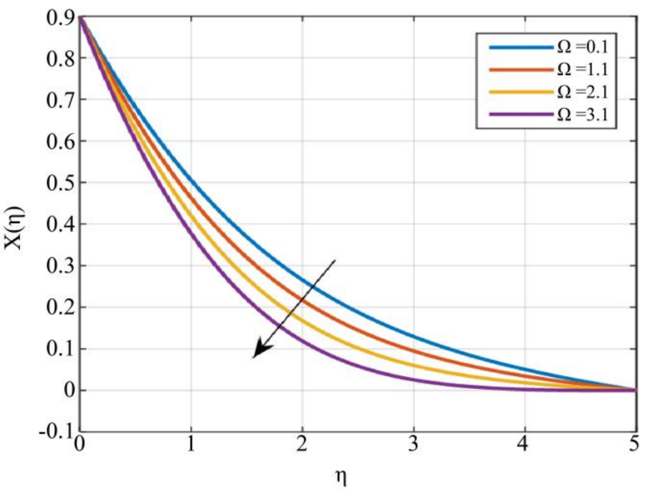

Fig. 24 Variations of Ω to $\chi(\eta)$

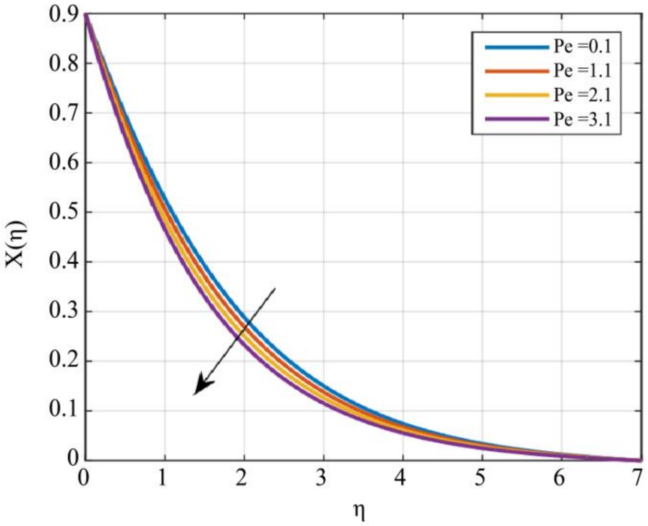

Fig. 22 Variations of Pe to $\chi(\eta)$

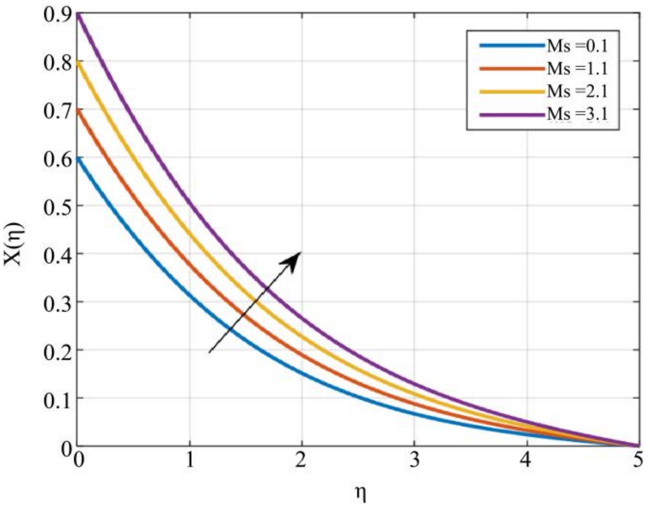

Fig. 25 Variations of Ms to $\chi(\eta)$

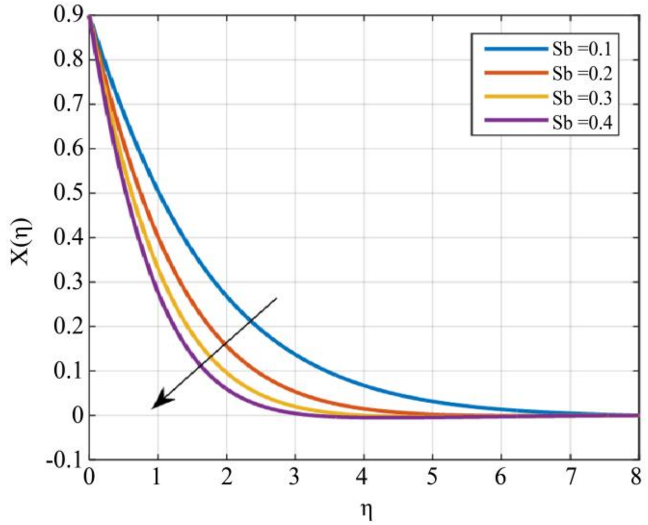

Fig. 23 Variations of Sb to $\chi(\eta)$

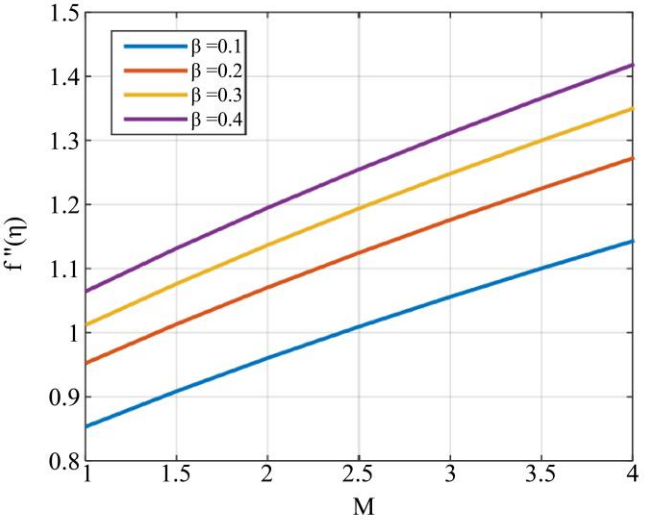

Fig. 26 Variations of M and β to $f''(0)$

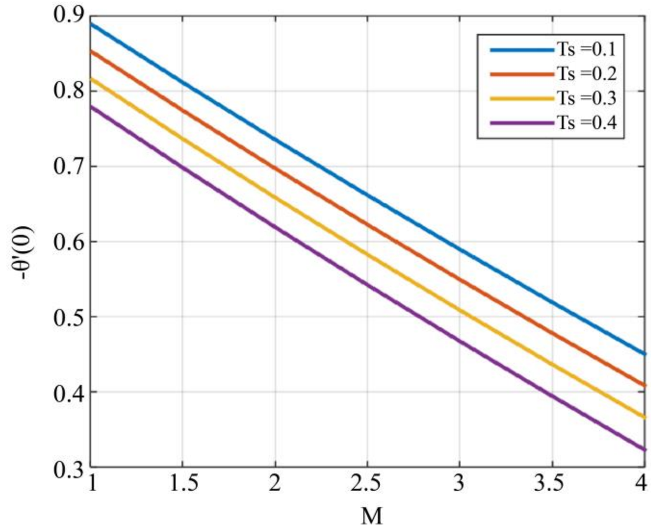

Fig. 27 Variations of M and Ts to $-\theta'(0)$

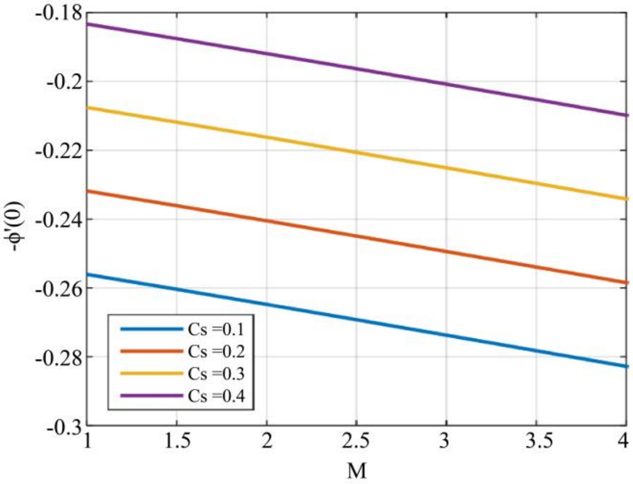

Fig. 28 Variations of Cs and M to $-\phi'(0)$

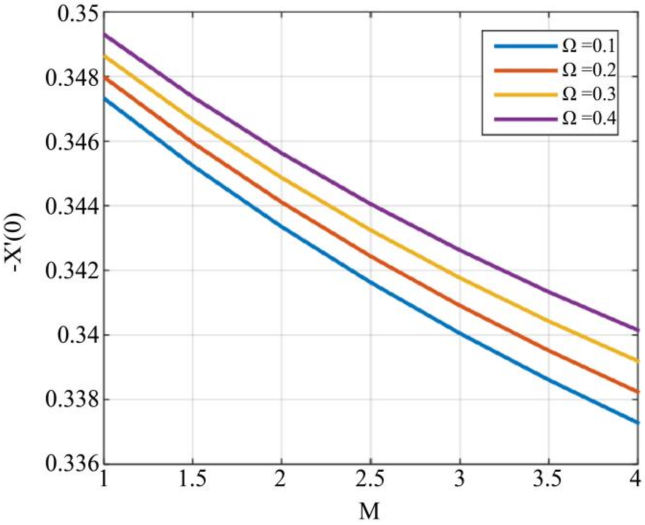

Fig. 29 Variations of M and Ω to $-\chi'(0)$

Figure 11 illustrates the temperature field influenced by thermal radiation. Fluid temperature increases thermal radiation due to the added heat it brings. Thermal radiation, being a mode of heat transfer by electromagnetic waves, increases energy exchange in the system. This contribution causes temperature gradients and differences in the system. Figure 12 illustrates the Prandtl number (Pr) influence on temperature variation. The reverse relationship — larger Pr retards heat diffusion and vice versa. Consequently, heat retention is enhanced and radiative heat transfer is reduced. The explanation also mentions the Eckert number, which also has an effect on the manner in which temperature varies.

Figure 13 shows that an elevated Eckert number results in higher thermal energy being trapped in the fluid. This is because increased frictional heating enhances the total temperature distribution of the system. Higher kinetic energy enhances the transformation of nano-thermal energy, enhancing redistribution as well as heat retention within the fluid. Temperature gradients influenced by the effect of the Eckert number in modelling the competition between kinetic energy dissipation and thermal energy production in the flow. Thus, the Eckert number considerably influences the distribution of thermal energy and temperature gradients in the fluid. Eckert number’s effect on temperature distribution is depicted in Figure 14. Temperature within the fluid drops as the stratification parameter (Ts) rises, reflecting the influence of thermal stratification on the temperature gradient. Gradient affects heat transfer processes, since thermal energy moves naturally from higher-temperature to lower-temperature areas, and thus affects the overall thermal structure of the fluid in terms of direction and magnitude of heat transfer.

Figure 15 illustrates the unique influence of Joule heating on temperature profile, to the fluid internal energy is supplied which lead the thicken thermal boundary layer due to increase in its temperature. Consequently, the temperature gradient decreases at the wall, and therefore, surface heat flux and heat transfer nearly disappear. Figure 16 graphically illustrates the effect of the Schmidt number (Sc) on concentration profiles. Concentration reduces with increasing Sc; this is mainly because of the inverse relationship between mass diffusivity and Schmidt number. Lower mass diffusivity causes the concentration boundary layer to be thinner, making the diffusion process more difficult. Consequently, mass transfer becomes less effective, and the surface concentration goes down.

Diagram 17 shows how rising Solutal Stratification (Cs) decreases concentration. This stratification increases the concentration gradient between the surface and the top plate, decreasing the overall concentration of the system by minimizing solute mixing. The effect of chemical reaction on fluid concentration is presented in Figure 18, which indicates that the curves of concentration increase when reaction rates increase. This is because increased concentrations of solute lead to increased collision frequencies, speeding up the reaction. How the dimensionless activation-energy parameter (E) and concentration distribution are related is depicted in Figure 19. The figure shows that as E increases, the concentration gradient is more evident. This indicates that increased activation energy speeds up the chemical process, increasing mass transfer and overall concentration.

Figure 20 illustrates the influence of the Brownian motion parameter Nb on the system. Thermal diffusion is improved as a result of the random motion of nanoparticles within the boundary layer, triggered by high Nb values. Proper prediction of concentration gradients in systems influenced by Brownian motion demands detailed knowledge of its inherent mechanisms. Brownian motion plays a crucial role in promoting diffusion, achieving equilibrium concentrations, improving mixing, and facilitating particle transport and dispersion in the fluid, factors that collectively influence the formation of concentration gradients. Figure 21 illustrates an inverse relationship between the thermophoretic parameter and mass transfer rate. As the thermophoretic parameter increases, the mass transference rate correspondingly declines. Concentration is reduced due to more movement of nanoparticles as a result of the intensified temperature gradient. A higher thermophoretic parameter amplifies temperature differences, thereby slowing mass transport.

The effect of Pe on the motile microorganism gradient is shown in Figure 22. It demonstrates that as Pe upsurges, the diffusion coefficient and profile of microorganism density throughout the entire thickness of the boundary stratum upsurge. It describes the motion of the fluid's constituents. It is discovered that the diffusivity of microbes increases as the Peclet number rises. Physically, the Peclet number increases cell propulsion speed, increasing the motile microorganism density. Consequently, as Pe values increase, so do the mobility and diffusivity of microorganisms. The bioconvection Schmidt number, defined as the ratio of microorganism diffusivity to fluid kinematic viscosity, significantly influences the motility field χ(η), as shown in Figure 23 by the decline in liquid motility with its increase. This number represents the balance between diffusion and advection in microorganism movement. Higher values specify diffusion dominance, in this case, rapid diffusion of microbes since their transport by fluid flow, resulting in clear bioconvection patterns.

Figure 24 explores the connection between the microorganism concentration difference constraint and the motile density of the fluid. Such bioconvective formations appear significantly owing to the predominant motion of microorganisms compared to bulk fluid flow. It indicates that the motile density diminishes with an increase in the parameter X. This implies that the concentration difference constraints play a critical role in determining the motile microorganisms' distribution and cause them to congregate closer to the ambient boundary layer. Consequently, this parameter determines the dynamics of bio-convective in the fluid. Figure 25 indicates that the fluid exhibits reduced microorganism density closer to its exterior compared to the enclosing liquid, indicating a stratified microbial distribution. This stratification creates well-defined vertical density gradients in the fluid. Figure 26 illustrates how the factor of drag force f" (0) is affected by two definite parameters, namely, M and β. The drag force parameter rises with the rise in values of M and β. This shows that an important role in increasing the surface drag encountered in the system is performed by these parameters. The change in the Casson fluid parameter β and the magnetic parameter M significantly affects the skin friction coefficient, denoted as f" (0), for boundary layer flow of a Casson fluid along a stretching surface. As the magnetic parameter M grows, the Lorentz force due to the imposed magnetic field causes a resistive force on the fluid flow, hence decreasing the velocity at the near-surface point and diminishing the velocity gradient at the wall, thus resulting in the reduction of f" (0). However, the Casson parameter β determines the non-Newtonian nature of the fluid; a smaller β indicates increased non-Newtonian (Casson) effects, i.e., more resistance to flow from the yield stress of the fluid, leading to decreased wall shear stress. As β increases, the fluid's behavior moves closer to that of a Newtonian fluid, lowering this resistance and increasing the shear rate near the surface, which causes an increase in f" (0). Thus, whereas increasing M will tend to damp down the fluid motion and lower the skin friction, increasing β will improve the flow behavior and increase the skin friction coefficient. Figure 27 describes the variation of the magnetic parameter M and the thermal stratification parameter Ts, which has a significant influence on the heat transfer rate at the surface, indicated by the reduced Nusselt number $-\theta'(0)$. With increasing magnetic parameter M, the induced magnetic field exerts a Lorentz force opposing the fluid flow, lessening the convective heat transport from the surface, hence resulting in a reduction of $-\theta'(0)$, or the wall heat transfer rate. On the other hand, thermal stratification by Ts means that the surrounding fluid temperature is not the same at every point on the surface. As the value of Ts increases (increased stratification), the gradient in temperature from the surface to the surrounding fluid decreases, weakening the thermal boundary layer and consequently reducing $-\theta'(0)$ further. In short, both increased magnetic field strength (M) and intensified thermal stratification (Ts) result in a decrease in surface heat transfer rate.

Figure 28 illustrates that the fluctuation of the chemical stratification parameter Cs and the magnetic parameter M significantly influences the reduced Sherwood number -ϕ' (0), which is the mass transfer rate at the surface. A rise in the magnetic parameter M increases the Lorentz force that acts opposite to the motion of the fluid, causing a decrease in the velocity and hence a decrease in the convective mass transport close to the surface. This leads to a reduction in -ϕ' (0), which signifies a lower mass transfer rate at the wall. In contrast, raising the chemical stratification parameter Cs corresponds to a higher concentration gradient in the surrounding fluid, which reduces the practical concentration difference between the surface and the surrounding fluid. This inhibits the diffusive mass transport, again resulting in a decrease in -ϕ’ (0). Hence, more intense magnetic field effects (greater M) and greater chemical stratification (greater Cs) work to decrease the surface mass transfer rate. Figure 29 shows that the local density number of motile microorganisms at the surface, $-\chi'(0)$, is greatly affected by the magnetic parameter M and the motile microorganism parameter Ω. As M increases, the magnetic field induces a Lorentz force opposing the fluid flow, thus inhibiting the upward convective transport of motile microorganisms and leading to a reduction in $-\chi'(0)$, i.e., fewer microorganisms are transported to the surface. In contrast, an increase in Ω enhances the bioconvective flow induced by the self-propelled motion of microorganisms, leading to their accumulation close to the surface and thus enhancing $-\chi'(0)$. Thus, magnetic effects tend to reduce microorganism concentration at the wall, while stronger Bioconvection enhances it.

4. Conclusion

This investigation examines the non-uniform heat sources or sinks effect on Casson nanofluids Bioconvection over an exponentially stretching sheet. The following conclusions are drawn,

- Increasing the bioconvection Rayleigh number and magnetic field intensity leads to a reduction in the fluid’s velocity.
- As the buoyancy ratio, Prandtl number, and thermal and solutal stratification parameters rise, the velocity profile starts at zero, reaches a peak, and then returns to zero.
- Higher values of solutal stratification lead to increased mass and heat transfer rates.
- For larger Eckert numbers, the heat transfer rate decreases. When the Eckert number is zero, the results correspond to a scenario without viscous dissipation.
- Skin friction is lower in hydrodynamic flow compared to hydromagnetic flow.
- By using applications of a non-uniform heat source/sink, an improvement in the temperature of Casson nanoparticles is measured.
- The chemical reaction and activation energy parameters have opposing effects on the concentration profile.
- Thermal stratification and radiation increase the fluid’s temperature, with the temperature gradient rising as thermophoresis, Brownian motion, and related parameters increase.
- The motile density field decreases with increasing values of the bioconvection Schmidt number and the Peclet number.

References

[1] Sébastien Galtier, *Introduction to Modern Magnetohydrodynamics*, Cambridge University Press, pp. 1-268, 2016. [Google Scholar] [Publisher Link]

[2] B.C. Sakiadis, “Boundary-Layer Behavior on Continuous Solid Surfaces: I. Boundary-Layer Equations for Two-Dimensional and Axisymmetric Flow,” *AIChE Journal*, vol. 7, no. 1, pp. 26-28, 1961. [CrossRef] [Google Scholar] [Publisher Link]

[3] Jacek Kierzenka, and Lawrence F. Shampine, “A BVP Solver Based on Residual Control and the MATLAB PSE,” *ACM Transactions on Mathematical Software*, vol. 27, no. 3, pp. 299-316, 2001. [CrossRef] [Google Scholar] [Publisher Link]

[4] L.E. Erickson, L.T. Fan, and V.G. Fox, “Heat and Mass Transfer on Moving Continuous Flat Plate with Suction or Injection,” *Industrial & Engineering Chemistry Fundamentals*, vol. 5, no. 1, pp. 19-25, 1966. [CrossRef] [Google Scholar] [Publisher Link]

[5] Stephen U.S. Choi, “Enhancing Thermal Conductivity of Fluids with Nanoparticles,” *International Mechanical Engineering Congress and Exposition, San Francisco*, California, USA, pp. 99-105, 1995. [CrossRef] [Google Scholar] [Publisher Link]

[6] Kaufui V. Wong, and Omar De Leon, “Applications of Nanofluids: Current and Future,” *Advances in Mechanical Engineering*, vol. 2, pp. 1-11, 2010. [CrossRef] [Google Scholar] [Publisher Link]

[7] A.V. Kuznetsov, “Non-Oscillatory and Oscillatory Nanofluid Bio-Thermal Convection in a Horizontal Layer of Finite Depth,” *European Journal of Mechanics B/Fluids*, vol. 30, no. 2, pp. 156-165, 2011. [CrossRef] [Google Scholar] [Publisher Link]

[8] A. Kamran et al., “A Numerical Study of Magnetohydrodynamics Flow in Casson Nanofluid Combined with Joule Heating and Slip Boundary Conditions,” *Results in Physics*, vol. 7, pp. 3037-3048, 2017. [CrossRef] [Google Scholar] [Publisher Link]

[9] Bharatkumar K. Manvi et al., “MHD Casson Nanofluid Boundary Layer Flow in Presence of Radiation and Non-Uniform Heat Source/Sink,” *Mathematical Modelling and Control*, vol. 3, no. 3, pp. 152-167, 2023. [CrossRef] [Google Scholar] [Publisher Link]

[10] Anum Naseem, and Abdul Ghafoor Kasana, “Numerical Assessment of MHD Hybrid Nanofluid Flow Over an Exponentially Stretching Surface in the Presence of Mixed Convection and Non-Uniform Heat Source/Sink,” *Results in Engineering*, vol. 22, pp. 1-14, 2024. [CrossRef] [Google Scholar] [Publisher Link]

[11] D. Gowri Shankar et al., “Cattaneo-Christov Heat Flux on an MHD 3D Free Convection Casson Fluid Flow Over a Stretching Sheet,” *Engineering Transactions*, vol. 68, no. 3, pp. 223-238, 2020. [CrossRef] [Google Scholar] [Publisher Link]

[12] M. Sudheer Babu, B. Reddappa, and S. Sreenadh, "Effect of Second Order Chemical Reaction and Double Stratification on MHD Free Convection Flow of Casson Fluid Over an Exponentially Stretching Sheet through Porous Medium," *Gorteria Journal*, vol. 35, no. 3, pp. 53-66, 2022. [Google Scholar]

[13] Hassan Waqas et al., "Numerical Simulation for Bioconvectional Flow of Burger Nanofluid with Effects of Activation Energy and Exponential Heat Source/Sink Over an Inclined Wall under the Swimming Microorganisms," *Scientific Reports*, vol. 11, pp. 1-15, 2021. [CrossRef] [Google Scholar] [Publisher Link]

[14] A.V. Kuznetsov, and A.A. Avramenko, "Effect of Small Particles on this Stability of Bioconvection in a Suspension of Gyrotactic Microorganisms in a Layer of Finite Depth," *International Communications in Heat and Mass Transfer*, vol. 31, no. 1, pp. 1-10, 2004. [CrossRef] [Google Scholar] [Publisher Link]

[15] Yun-Xiang Li et al., "Dynamics of Casson Nanoparticles with Non-Uniform Heat Source/Sink: A Numerical Analysis," *Ain Shams Engineering Journal*, vol. 13, no. 1, pp. 1-8, 2022. [CrossRef] [Google Scholar] [Publisher Link]

[16] Yun-Jie Xu et al., "Effectiveness of Induced Magnetic Force and Non-Uniform Heat Source/Sink Features for Enhancing the Thermal Efficiency of Third Grade Nanofluid Containing Microorganisms" *Case Studies in Thermal Engineering*, vol. 27, pp. 1-10, 2021. [CrossRef] [Google Scholar] [Publisher Link]

[17] G. Vinod Kumar et al., "Unsteady Magnetohydrodynamic Nanofluid Flow Over a Permeable Exponentially Surface Manifested with Non-Uniform Heat Source/Sink Effects," *Waves in Random and Complex Media*, vol. 35, no. 3, pp. 5651-5669, 2022. [CrossRef] [Google Scholar] [Publisher Link]

[18] Sharanayya, and Suresh Biradar, "Magnetized Dissipative Casson Nanofluid Flow over a Stretching Sheet with Heat Source/Sink and Soret Effect under Porous Medium," *BioNanoScience*, vol. 13, pp. 2103-2121, 2023. [CrossRef] [Google Scholar] [Publisher Link]

[19] R. Mahesh et al., "Impact of Radiation on the MHD Couple Stress Hybrid Nanofluid Flow over a Porous Sheet with Viscous Dissipation," *Results in Engineering*, vol. 17, pp. 1-12, 2023. [CrossRef] [Google Scholar] [Publisher Link]

[20] S.R.R. Reddy, and P.B.A. Reddy, "Impact of Thermal Radiation and Viscous Dissipation on Hydromagnetic Unsteady Flow Over an Exponentially Inclined Preamble Stretching Sheet," *Journal of Computational & Applied Research in Mechanical Engineering*, vol. 10, no. 1, pp. 171-181, 2020. [CrossRef] [Google Scholar] [Publisher Link]

[21] M. Siva Sankari et al., "Analytical Analysis of the Double Stratification on Casson Nanofluid Over an Exponential Stretching Sheet," *Case Studies in Thermal Engineering*, vol. 50, pp. 1-14, 2023. [CrossRef] [Google Scholar] [Publisher Link]

[22] M. Siva Sankari et al., "Homotopic Analysis for Bioconvection of Casson Nanofluid Flow Over an Exponential Stretching Sheet with Activation Energy and Motile Microorganism," *Numerical Heat Transfer, Part A: Applications*, vol. 86, no. 16, pp. 5603-5625, 2024. [CrossRef] [Google Scholar] [Publisher Link]

[23] Y. Vinod et al., "Boundary Layer Flow of a Non-Newtonian Fluid over an Exponentially Stretching Sheet with the Presence of a Heat Source/Sink," *Partial Differential Equations in Applied Mathematics*, vol. 13, pp. 1-14, 2025. [CrossRef] [Google Scholar] [Publisher Link]